Interpreting Seasonal and Interannual Hadley Cell Descending Edge Migrations via the Cell-Mean Rossby Number

SPENCER A. HILL,[a] SIMONA BORDONI,[b] JONATHAN L. MITCHELL,[c,d] AND JUAN M. LORA[e]

[a] *Department of Earth and Atmospheric Sciences, City College of New York, New York, New York*
[b] *Department of Civil, Environmental and Mechanical Engineering (DICAM), University of Trento, Trento, Italy*
[c] *Department of Earth, Planetary, and Space Sciences, University of California, Los Angeles, Los Angeles, California*
[d] *Department of Atmospheric and Oceanic Sciences, University of California, Los Angeles, Los Angeles, California*
[e] *Department of Earth and Planetary Sciences, Yale University, New Haven, Connecticut*

(Manuscript received 3 December 2024, in final form 16 April 2025, accepted 16 May 2025)

ABSTRACT: The poleward extent of Earth's zonal-mean Hadley cells varies across seasons and years, which would be nice to capture in a simple theory. A plausible, albeit diagnostic, candidate from Hill et al. combines the conventional two-layer, quasigeostrophic, baroclinic instability-based framework with a less conventional assumption that each cell's upper-branch zonal winds are suitably captured by a single, cell-wide Rossby number, with meridional variations in the local Rossby number neglected. We test this theory against ERA5 reanalysis data, finding that it captures both seasonal and interannual variations in the Hadley cell zonal winds and poleward extent fairly well. For the seasonal cycle of the Northern Hemisphere (NH) cell poleward edge only, this requires empirically lagging the prediction by 1 month, for reasons unclear to us. In all cases, the bulk Rossby number value that yields the most accurate zonal wind fields is approximately equal to the actual, diagnosed cell-mean value. Variations in these cell-mean Rossby numbers, in turn, predominantly drive variations in each cell's poleward extent. All other terms matter much less—including the subtropical static stability, which, by increasing under global warming, is generally considered the predominant driver of future Hadley cell expansion. These results argue for developing a predictive theory for the cell-mean Rossby number and for diagnosing its role in climate model projections of future Hadley cell expansion.

KEYWORDS: Dynamics; Hadley circulation; Reanalysis data; Interannual variability; Seasonal cycle

1. Introduction

Descent in the poleward branches of the time-mean, zonal-mean Hadley cells promotes aridity in the subtropics, fundamentally shaping Earth's hydrological cycle. How far this descent spans poleward, and why, motivated foundational studies of Earth's general circulation (Halley 1686; Hadley 1735; Ferrel 1856) and remains actively investigated. In both hemispheres, it contracts equatorward in winter to spring and expands poleward in summer to autumn; interannually, it tends to contract equatorward in the warm, El Niño phase of El Niño–Southern Oscillation (ENSO) and to expand poleward in the cool, La Niña phase, though more reliably for the Southern Hemisphere (SH) than the Northern Hemisphere (NH) (Caballero 2007; Lu et al. 2008; Tandon et al. 2013; Zurita-Gotor and Álvarez-Zapatero 2018; Seo et al. 2023). Here, we show that a simple theory captures these seasonal and interannual migrations in reanalysis data fairly well and is likely applicable in other contexts, such as the cells' poleward expansion under global warming (e.g., Vallis et al. 2015; Chemke and Polvani 2019; Staten et al. 2020).

Dynamically, each hemisphere's poleward Hadley cell edge demarcates the transition between the extratropics, which are strongly influenced by large-scale baroclinic eddies, and the tropics, where those baroclinic eddies are much less prevalent (Showman et al. 2014)—making it natural to link the edge's location to where baroclinic instability first sets in (Held 2000; Kang and Lu 2012; Hill et al. 2022; Peles and Lachmy 2023). In the influential model introduced by Held (2000), this is determined by where the upper-layer westerlies of the Hadley cells exceed the critical speed for baroclinic instability according to a simple, two-layer, quasigeostrophic model. On a given planet with fixed gravitational constant, planetary radius, and planetary rotation rate, the two terms that can change this critical zonal wind field are the tropopause height and the static stability, and prior studies have affirmed the predominance of the subtropical static stability in warming-induced Hadley cell expansion (e.g., Chemke and Polvani 2019).

For the given values of these two parameters and thus of the critical zonal wind field, the onset latitude still depends on the Hadley cell upper-branch zonal wind field, which Held (2000) took as the angular momentum conserving zonal winds with ascent at the equator (Held and Hou 1980). But the same baroclinic eddies, by propagating equatorward and breaking within the Hadley cells, decelerate winds well below this limit (Walker and Schneider 2005, 2006; Schneider 2006; Sobel and Schneider 2009). So too do migrations of the Hadley cell *ascending* edge off the equator, by reducing the planetary angular momentum value imparted to the free troposphere (Kang and Lu 2012; Hilgenbrink and Hartmann 2018; Watt-Meyer and Frierson 2019), as occurs seasonally when the ascending branch expands into either summer hemisphere (Lindzen and Hou 1988). The decelerations by either mechanism, in turn, move the baroclinic instability onset latitude poleward. These factors—a descending edge determined by baroclinic instability onset and Hadley cell zonal wind fields that depend on both the

Corresponding author: Spencer A. Hill, shill1@ccny.cuny.edu

DOI: 10.1175/JCLI-D-24-0678.1

aggregate extratropical eddy stresses and ascending edge migrations—have been formalized by Hill et al. (2022), drawing heavily from Kang and Lu (2012).

A central ansatz of the Hill et al. (2022) theory is that the local Rossby number, a scalar formally defined below that essentially quantifies the strength of the eddy stresses at each latitude, is uniform within each Hadley cell's upper branch at any given time and consequently that each Hadley cell's upper-branch zonal winds are suitably approximated by those required by a uniform Rossby number. Crucially, this cell-mean Rossby number value can differ between the NH and SH cells at any particular time and for either cell can vary in time, such as seasonally or interannually (e.g., Schneider 2006; Bordoni and Schneider 2008; Kang and Lu 2012). Our purpose here is to test that ansatz and the theory's broader fidelity for Earth's current climate, as represented in reanalysis data. After formally presenting the theory (section 2) and methodological choices (section 3), we show that, unsurprisingly (e.g., Schneider 2006; Caballero 2007; Singh 2019), the Rossby number is far from uniform within either Hadley cell almost always but that, more surprisingly, the uniform Rossby number zonal wind fields nevertheless capture the actual wind fields quite well, both for the climatological seasonal cycle (section 4) and interannual variability (section 5). Moreover, the theory captures the Hadley cell descending edges fairly well in both contexts. Several prior studies affirm the central role in reanalysis data of variations in eddy stresses on variations of the Hadley cells interannually (Caballero 2007; Zurita-Gotor and Álvarez-Zapatero 2018; Seo et al. 2023). More recently, Peles and Lachmy (2023) have done so for the climatological seasonal cycle, showing for both hemispheres in JRA-55 data that multiple bulk measures of the equatorward extent of baroclinic instability track the climatological seasonal cycle of the Hadley cell well. In effect, the present study seeks to further distill these prior results into the simplest plausible analytical framework and then use that framework to evaluate the relative importance of each term appearing—the cell-mean Rossby number, the ascending edge latitude, the static stability, and the tropopause height—finding the cell-mean Rossby number to predominantly control the Hadley cell descending edge migrations both seasonally and interannually. We conclude by discussing some implications of these results, including for forced Hadley cell expansion under global warming (section 6).

2. Theory

The theory was originally presented by Hill et al. (2022) and draws heavily from Kang and Lu (2012). The local Rossby number is

$$\mathrm{Ro}(\varphi) \equiv -\frac{\zeta}{f}, \tag{1}$$

where φ is the latitude, $\zeta \equiv (a\cos\varphi)^{-1}\partial_\varphi(u\cos\varphi)$ is the zonal-mean relative vorticity with zonal-mean zonal wind u, and $f \equiv 2\Omega\sin\varphi$ is the planetary vorticity. In what follows, u and all other fields are taken to be monthly or longer averages.

If the local Rossby number is meridionally uniform, $\mathrm{Ro}(\varphi) \equiv \mathrm{Ro}$, then integrating (1) meridionally yields the uniform Rossby number zonal wind field:

$$u_{\mathrm{Ro}}(\varphi;\,\mathrm{Ro},\,\varphi_\mathrm{a}) = \mathrm{Ro}\,u_{\mathrm{amc}}(\varphi;\,\varphi_\mathrm{a}) = \mathrm{Ro}\,\Omega a\left(\frac{\sin^2\varphi - \sin^2\varphi_\mathrm{a}}{\cos\varphi}\right), \tag{2}$$

where u_{amc} is the angular momentum conserving zonal wind field, given the ascending edge φ_a (Held and Hou 1980; Lindzen and Hou 1988). As the ascent moves away from the equator, a smaller planetary vorticity value is advected into the free troposphere, causing the resulting uniform Ro zonal winds to be less westerly at all latitudes. The angular momentum conserving solution amounts to the limiting case of $\mathrm{Ro} = 1$.

Meanwhile, the critical upper-level zonal wind for baroclinic instability in the two-layer quasigeostrophic model is given by

$$u_{\mathrm{BCI}}(\varphi;\,H,\,\Delta_\mathrm{v}) = \frac{gH\Delta_\mathrm{v}}{2\Omega a}\frac{\cos\varphi}{\sin^2\varphi}, \tag{3}$$

where g is the gravity, H is the tropopause height, Ω is the planetary rotation rate, a is the planetary radius, and Δ_v is a dimensionless bulk static stability.[1] More precisely, this is an expression for the critical vertical shear in the zonal wind, but we assume as standard that the lower-layer zonal wind magnitude is negligible (Held 2000).

We then solve for the latitude where instability first sets in by setting $u_{\mathrm{Ro}} = u_{\mathrm{BCI}}$. Equating the right-hand sides of (2) and (3), the result in the small-angle limit is

$$\varphi_\mathrm{d}^2 = c_\mathrm{d}^2\left(\frac{\varphi_\mathrm{a}^2}{2} + \sqrt{\frac{\varphi_\mathrm{a}^4}{4} + \frac{\mathrm{Bu}\Delta_\mathrm{v}}{2\mathrm{Ro}}}\right), \tag{4}$$

where

$$\mathrm{Bu} \equiv \frac{gH}{(\Omega a)^2} \tag{5}$$

is the planetary Burger number, and we have also introduced a near-unity empirical fitting constant, c_d: Denoting the true solution as φ_{BCI}, we set $\varphi_\mathrm{d} \equiv c_\mathrm{d}\varphi_{\mathrm{BCI}}$. In (4), the Rossby number is what encapsulates the deceleration of the Hadley cell zonal winds by extratropical eddy stresses. We will show that it can be interpreted as a meridional average of the local Rossby number within the upper branch of each Hadley cell. From (4), the descending edge moves poleward as Ro decreases or φ_a moves poleward. Only the absolute value of the ascending edge, $|\varphi_\mathrm{a}|$ rather than φ_a, influences the descending edge prediction, a consequence of the symmetry about the equator of u_{Ro}: $u_{\mathrm{Ro}}(\varphi;\,\mathrm{Ro},\,\varphi_\mathrm{a}) = u_{\mathrm{Ro}}(|\varphi|;\,\mathrm{Ro},\,|\varphi_\mathrm{a}|)$. In other

[1] Note that Hill et al. (2022) mistakenly omit the factor of 2 in the denominator of (3). Fortunately, this does little damage to the resulting prediction for the descending edge because the missing $2^{-1/4} \approx 0.84$ constant factor that results in the descending edge prediction can implicitly be subsumed into the empirical fitting constant c_d, whose precise value is already not taken seriously.

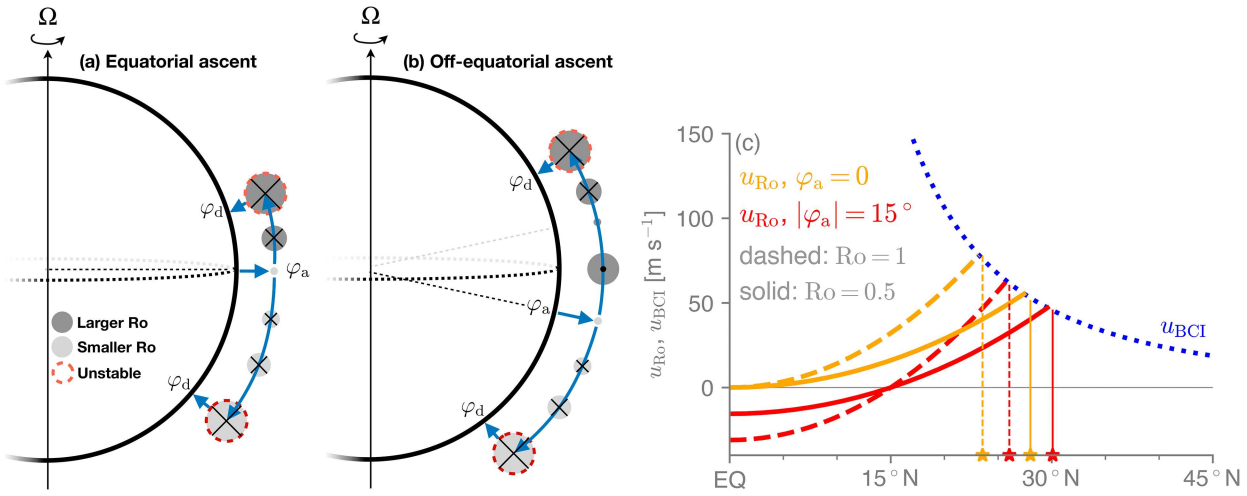

FIG. 1. Schematic of the influences of the mean upper-tropospheric Rossby number in each Hadley cell, Ro, as well as the ascent latitude, φ_a, on the latitude of the descending edge, φ_d, according to our theory. In (a) and (b), blue arrows signify the locations of ascent, descent, and the directions of the meridional flow in each cell's upper branch, and the cell-mean Rossby number is smaller for the SH cell compared to the NH cell, enabling the SH cell to extend farther poleward before its zonal winds (gray circles with black Xs for westerlies or dots for easterlies, with larger symbols indicating larger magnitudes) become baroclinically unstable, thereby causing the cell to terminate. In (b), ascent is off the equator, which compared to the corresponding on-equatorial-ascent case in (a) results in less westerly zonal winds and thus further poleward Hadley cell extents. (c) Uniform Rossby number zonal wind fields, u_{Ro}, with either (orange) equatorial ascent or (red) ascent at 15°N or S, each with either (dashed) Ro = 1 or (solid) Ro = 0.5. The dotted blue line is u_{BCI}, the critical zonal wind for baroclinic instability, using $\Delta_v = 1/8$, $H = 10$ km, and standard values of all other constants. Stars and vertical lines at the intersections of the u_{Ro} fields with u_{BCI} signify the prediction for the descending edge φ_d for that u_{Ro}.

words, whether the ascent is in the Northern or Southern Hemisphere does not matter; what matters is how far poleward it is into either hemisphere. These behaviors are shown schematically in Fig. 1. Absent from Fig. 1 are the influences of changes in H and Δ_v. Both move the descending edge prediction poleward as they increase, all else equal, but as shown below, they play negligible roles in the seasonal cycle and interannual variability.

Though Hill et al. (2022) combine (4) with a separate theory that predicts the ascending edge latitude based on the extent of tropical supercriticality (Hill et al. 2021), we find the abrupt jumps of the ascending edge over the seasonal cycle predicted therein to be inconsistent with the more nearly sinusoidal seasonality in the ascending edge in reanalysis data shown below (Dima and Wallace 2003)—which is likely strongly influenced by zonally asymmetric eddies (Walker and Schneider 2005; Schneider and Bordoni 2008; Geen et al. 2019) in addition to thermal inertia (Wei and Bordoni 2018; Zhou and Xie 2018). We therefore proceed using (4) and emphasize that this is a diagnostic expression, lacking as we do compelling predictive theories for either the ascending edge latitude or the cell-mean Rossby number.

In the case of on-equatorial ascent, $\varphi_a = 0$, (4) simplifies to

$$\varphi_{d,0} \equiv \varphi_d(\varphi_a = 0) = c_d\left(\frac{\mathrm{Bu}\Delta_v}{2\mathrm{Ro}}\right)^{1/4}, \tag{6}$$

from which one sees that, once the c_d constant is distributed through, the last term in (4) is equivalent to $\varphi_{d,0}^4$. The expression (6) reduces to the original Held (2000) expression in the Ro = 1, angular momentum-conserving limit.

As Held (2000) notes, some of the two-layer quasigeostrophic assumptions are tenuous when applied to the real atmosphere, and more recently, Peles and Lachmy (2023) nicely summarize and expand upon the class of approaches that incorporate more comprehensive physics. In particular, in continuously stratified atmospheres, no critical shear exists that determines baroclinic instability onset, and prior studies (Korty and Schneider 2008; Levine and Schneider 2011, 2015) have instead framed the eddy influence on the cell edges in terms of extratropical supercriticality, a measure of the vertical extent of eddy heat fluxes within the troposphere (Held 1978). Also, arguably, the Hadley cell descending edges depend less directly on the location of wave generation, which the instability criterion nominally corresponds to, than on the location of wave breaking (Vallis et al. 2015), which in turn is not even a single latitude, varying as it does with the eddy phase speed (e.g., Chen and Held 2007). Finally, despite considerable theoretical, modeling, and reanalysis-based evidence that extratropical eddy processes do fundamentally control the Hadley cell descending edge latitudes, the causality has recently been questioned, at least in the context of warming-induced poleward expansion (Davis and Birner 2022). The reader should keep these important caveats in mind as we proceed in using the simple metric (4) to predict φ_d.

3. Methods

a. Reanalysis data

We use monthly fields from the European Center for Medium-Range Weather Forecasts (ECMWF) ERA5 reanalysis

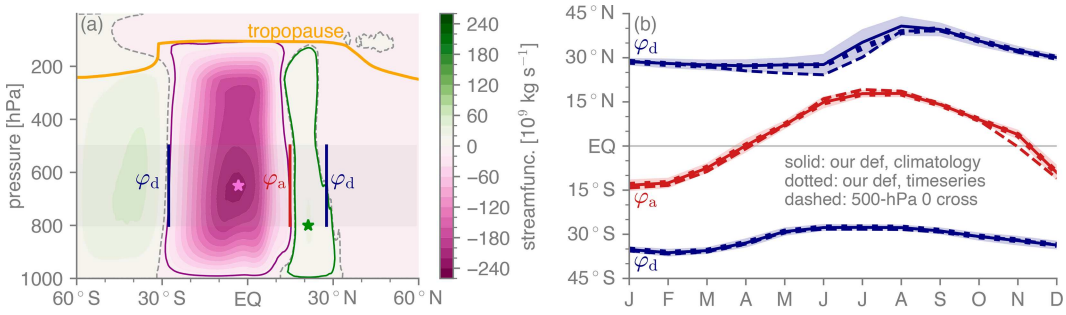

FIG. 2. (a) For the June climatology, meridional mass streamfunction in color shading according to the color bar. The 500–800-hPa layer is shaded gray, and our diagnosed cell edges are overlaid over that span at their latitudes. Pink and green stars show the SH and NH cell center locations, respectively. Solid purple and green curves are 5% of the SH and NH Hadley cell maxima, respectively, and dashed gray curves are the streamfunction zero crossings. The orange curve is the local tropopause. (b) Diagnosed monthly climatological Hadley cell edges. Solid lines use the streamfunction for each calendar month climatology averaged over 500–800 and using a 5% threshold from the center. Dotted lines are the same but applied to each individual month and then averaged across years. Dashed lines are the conventional 500-hPa zero crossing applied to the monthly climatologies. Shading shows the ±1 interannual standard deviation range for our 500–800-hPa-based metric.

dataset (Hersbach et al. 2020) spanning from January 1979 to December 2023. These are provided by ECMWF transformed from the underlying numerical model's native coordinate system to a 0.25° × 0.25° latitude–longitude horizontal grid and to 37 fixed pressure levels from 1000 to 1 hPa in the vertical. We compute annual, seasonal, and calendar-month climatologies over 1979–2023, as well as time series of fields averaged over each calendar year.

b. *Standard Hadley cell diagnostics*

As standard, the starting point for our Hadley cell diagnostics is the Eulerian-mean meridional mass overturning streamfunction, Ψ:

$$\Psi(\varphi, p) = 2\pi a \cos\varphi \int_0^p v \frac{\mathrm{d}p'}{g}, \tag{7}$$

where a is the planetary radius, φ is the latitude, p is the pressure, v is the zonal-mean meridional wind, and g is the gravitational acceleration. It is signed such that the SH Hadley cell is negative and the NH cell is positive. Though not shown in (7), as standard at each latitude, the column average of v is subtracted from v at all levels barotropically to enforce vanishing column-integrated mass transport and thus that Ψ vanishes at the upper and lower boundaries.

Rather than the conventional zero crossing of the 500-hPa streamfunction (e.g., Adam et al. 2018), the descending edge latitudes are diagnosed as where the streamfunction vertically averaged over 500–800 hPa decreases to 5% of its value at the center, linearly interpolating between the two grid points bracketing this threshold crossing. The ascending edge is defined in the same way, moving northward from the SH cell center, and the cell center is defined as the latitude and pressure where the streamfunction takes its maximum magnitude within a given Hadley cell.

Figure 2a illustrates the factors motivating these choices using the month of June. An average over the 500–800-hPa layer (gray shading) is chosen as a compromise between the conventional 500-hPa level and the fact that, except for the NH cell in April and May, the cell maximum strengths all occur at or vertically below 600 hPa (pink and green stars for June; not shown for other months). The choice of a 5% threshold rather than a true zero crossing is primarily motivated by the NH cell being very weak during the boreal summer months (e.g., Watt-Meyer et al. 2019): The SH cell strength exceeds that of the NH by more than tenfold in each of the June–August calendar month climatologies, the JJA seasonal-mean climatology, and in multiple boreal-summer months in 36 of the 45 years (not shown). As such, in some individual boreal summer months, the NH Hadley cell is so weak and poorly organized that the SH cell, rather than passing sharply through zero, gradually tails off moving northward, making zero crossing definitions of both the ascending and NH descending edge unphysical.

As one additional consideration—though admittedly not one directly relevant to our results—the 5% threshold constitutes a meaningful boundary of each Hadley cell in all directions, as shown by the overlaid solid purple and green contours in Fig. 2a, which is not true of the zero crossing shown in dashed gray contours. In particular, the 5% threshold for the SH cell is nearly coincident with the tropopause (overlaid orange curve, defined further below), consistent with the Hadley cells being confined to the troposphere.

Figure 2b shows the climatological seasonal cycles of all three edges and illustrates their metric and sampling sensitivities. Solid curves use our methods computed from the climatological streamfunction for each calendar month. Dotted curves are the same but computed for each individual month and then averaged for each calendar month across years. Because locating the cell center and threshold crossings are not linear operations, in principle, this choice of order of operations could matter (Adam et al. 2018), but in practice, it makes little difference here. More substantive differences, though still modest overall, arise from using the conventional 500-hPa zero

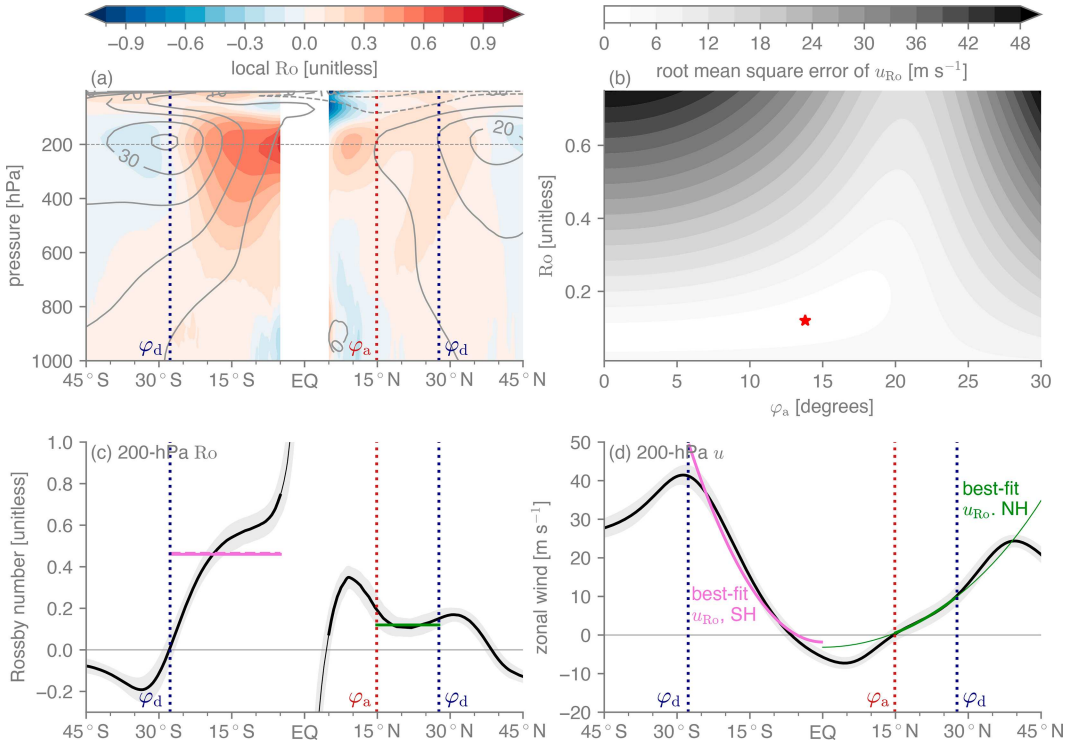

FIG. 3. For the ERA5 1979–2023 June climatology, (a) local Rossby number at each latitude and pressure in color shading according to the color bar and masked within 5°S–5°N, with local zonal wind overlaid in gray contours, with zero and positive values solid, negative dashed, and a 10 m s^{-1} contour interval. A thin horizontal line highlights the 200-hPa level. (b) RMSE of the uniform Rossby number zonal wind field for the June NH cell as a function of the selected Rossby number and ascent latitude, with the red star indicating the minimum, from which the best-fit Rossby number and ascent latitudes are selected. Meridional profiles at 200 hPa of (c) local Rossby number and (d) zonal wind in black, with shading showing ±1 interannual standard deviation. In (a), (c), and (d), dotted vertical lines show the three diagnosed Hadley cell edge latitudes. In (c), the thin black shows the values within 5°S–5°N where the Rossby number becomes ill behaved, and pink and green horizontal lines show the diagnosed (solid) and best-fit (dashed) cell-mean Rossby numbers, with the meridional span indicating the region over which they are calculated. In (d), pink and green curves show best-fit uniform Ro zonal wind fields for the SH and NH Hadley cells, respectively.

crossing metric, shown in dashed curves. The ascending edge defined this way moves southward across the equator more rapidly in November–December, and the NH descending edge is more equatorward by a few degrees in boreal spring through summer. From Fig. 2a for June at least, we see this stems from the bounding streamline of the NH cell tilting equatorward with height in the lower free troposphere. Finally, shading about the solid curves in Fig. 2b shows the ±1 interannual standard deviation range for our 500–800-hPa-based metric. For reasons just discussed, it is largest in the NH during boreal summer, but still for all three edges, it is modest relative to the seasonally forced climatological progression.

c. *Uniform Ro framework diagnostics*

Figure 3 uses the results for the June climatology to illustrate our methodology for constructing the uniform Rossby number fields. We start by computing the local Rossby number Ro(φ) at each latitude and pressure using (1), masking out values within 5°S–5°N where Ro(φ) $\propto 1/\sin\varphi$ becomes ill-defined (Fig. 3a).

We then compute each Hadley cell's cell-mean Rossby number Ro as an area-weighted meridional average of Ro(φ) at 200 hPa, which is the tropospheric level where it invariably maximizes (Fig. 3a). These span from that cell's diagnosed φ_d to whichever is closer: φ_a or 5° in the same hemisphere as φ_d, a choice again motivated by Ro(φ) being illdefined near the equator (Fig. 3c). As such, for cross-equatorial cells, this does not include the portion in the opposite hemisphere.

We fit u_{Ro} to each Hadley cell via a two-dimensional parameter sweep over Ro and φ_a, selecting the (Ro, φ_a) pair that minimizes the root-mean-square error (RMSE) of u_{Ro} against the climatological zonal wind at 200 hPa, over the same meridional span as just described for the cell-mean Rossby number, except with no masking near the equator (Fig. 3b for the June NH cell; June SH cell and all others not shown). For the climatological seasonal cycle, the sweep spans $0.01 \le \text{Ro} \le 0.75$ in 0.01 increments and $0° \le \varphi_a \le 30°$ in 0.1° increments. For interannual variability, where variations in both fields are smaller, the sweep spans $0.2 \le \text{Ro} \le 0.4$ in 0.002 increments and $0° \le \varphi_a \le 15°$ in 0.1° increments. The

RMSE of the u_{Ro} fields is generally more sensitive to the specified Rossby number than to the ascent latitude.

This procedure yields for each cell a best-fit u_{Ro} field (Fig. 3d) and corresponding best-fit values of Ro and φ_a. To interpret the physical significance of these four best-fit values, we compare them to their directly diagnosed counterparts: the two diagnosed cell-mean Ro values and the single diagnosed φ_a value as discussed further below.

We compute the tropopause height at each latitude, $H(\varphi)$, using the standard lapse-rate-based definition as the lowest point where the local lapse rate drops below 2 K km^{-1} (WMO 1957), first refining the vertical resolution via cubic interpolation to 0.1-hPa-spaced levels. The resulting $H(\varphi)$ field is very flat within the tropics, has a sharp gradient always poleward of the Hadley cell descending edges by a few degrees, and in the extratropics slopes more gradually down moving poleward. We compute the bulk static stability at each latitude, $\Delta_v(\varphi)$, as the difference between the potential temperature at 500 and 850 hPa, divided by a standard reference value of 300 K: $\Delta_v(\varphi) \equiv [\theta_{500}(\varphi) - \theta_{850}(\varphi)]/\theta_{ref}$. Climatologically, across all calendar months and nonpolar latitudes, this ranges over ~0.055–0.085. The specific levels of 500 and 850 hPa follow Lu et al. (2008), motivated by eddy growth being more sensitive to lower- than upper-tropospheric baroclinicity. As a sensitivity test, using 300 rather than 500 hPa as the upper level does not strongly influence our results (not shown).

In the two-layer, quasigeostrophic model underlying the baroclinic instability onset criterion, the tropopause height and bulk static stability are fixed, global constants, and only by treating them as such can (4) be derived. But in the real atmosphere, they vary nontrivially in space and time, and for the tropopause, these variations are clearly strongly influenced by the extent of the Hadley cells, as can be inferred from Fig. 2 for June. We therefore create bulk midlatitude values for each by meridionally averaging each over the 20° latitude span of the extratropics beginning 5° poleward of the Hadley cell descending edge. As shown below, neither term strongly influences the Hadley cell descending edge predictions anyway, making this theoretical ambiguity not of practical importance.

We set the empirical fitting constant c_d to a fixed value for each hemisphere, in each case chosen subjectively to provide, by eye, the best overall fit across all months for the climatological seasonal cycle or years for interannual variability. For the seasonal cycle, these are 1.04 for the NH and 1.09 for the SH; for interannual variability, they are 1.02 for the NH and 1.09 for the SH. Given sampling and metric uncertainties—consider, for example, that the reference temperature of 300 K in the denominator of Δ_v is somewhat arbitrary—and that the resulting values all end up being near unity, we do not consider the specific values of c_d as being particularly meaningful; see Hill et al. (2022) for further discussion.

For interannual variability, we compute yearly values of the Niño-3.4 index over 1979–2023 using monthly data from the NOAA Extended Reconstructed sea surface temperature (ERSST), version 4, dataset (Huang et al. 2015). Niño-3.4 is defined as the average SST anomaly spanning 120°–170°W, 5°S–5°N. All correlation coefficients are computed on detrended fields, with trends computed over 1979–2023 via linear regression and then subtracted off. Regarding statistical significance, autocorrelations are small for all fields examined (not shown), justifying approximating each year of the 45-yr record as independent. The resulting threshold correlation coefficient magnitude for the $p = 0.05$ significance level is 0.29.

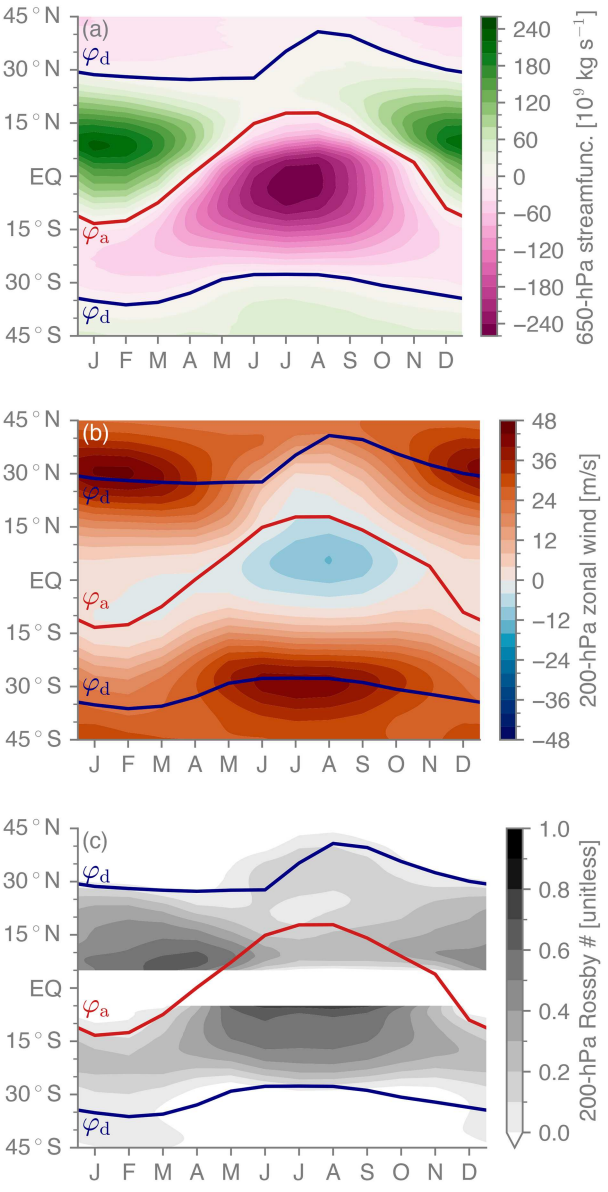

FIG. 4. In solid curves in each panel, the Hadley cell ascending edge in dark red and the descending edges in dark blue. In color shading, climatological seasonal cycles of (a) meridional mass overturning streamfunction at 650 hPa and at 200 hPa of (b) zonal wind and (c) the local Rossby number, with values in (c) masked out within 5° of the equator where the denominator approaches zero.

4. Seasonal cycle

Figure 4a shows the climatological seasonal cycles of both the descending edge and the ascending edge. The SH descending

edge ranges from 27.6°S in July to 36.2°S in February, and the NH descending edge ranges from 27.3°N in April to 40.8°N in August. The ascending edge varies smoothly between 13.3°S in January and 17.9°N in August, lagging the insolation by ~1 month owing to the coupled surface–lower atmosphere system's thermal inertia (e.g., Mitchell et al. 2014).

These seasonal migrations in the cell edges occur in concert with changes in the rate of mass overturned within the cells, shown as filled contours in Fig. 4a, with either cell's mass overturning strengthening from that hemisphere's autumn into winter as it grows meridionally and becomes crossequatorial and subsequently contracting and weakening in local spring through summer. Peak mass overturning rates, exceeding 240×10^9 kg s^{-1}, occur at and just south of the equator in austral winter within the center of the cross-equatorial cell.

Figure 4b shows the climatological monthly zonal-mean zonal wind at 200 hPa. It is easterly at the equator except in boreal winter (Zhang and Lutsko 2022). Within the meridional extent of the Hadley cells, the easterlies peak in meridional extent and magnitude—respectively, ~10°S–20°N and ~12 m s^{-1}—in boreal summer within the strong, cross-equatorial cell (Bordoni and Schneider 2008). In every month, winds monotonically become more positive moving poleward from their deep-tropical minimum, reaching ~40 m s^{-1} at the descending edge of either winter, cross-equatorial cell. The 200-hPa zonal wind is small in the vicinity of the ascending edge in all months, which coheres qualitatively with the assumption of vanishing zonal wind there in our theory.

Figure 4c shows the climatological monthly mean local Rossby number at 200 hPa, masked out within 5° latitude of the equator where it is ill defined. It has a more complicated meridional structure than the zonal wind itself, though throughout the year in both hemispheres it is small, ~0–0.2, in the vicinity of the descending edge. It reaches up to ~0.7 within either winter, cross-equatorial cell, supported by a reinforcing feedback: ascent moving poleward increases the extent and magnitude of upper-tropospheric easterlies, which in turn prevents extratropical-origin eddies from breaking over more of the tropics, enabling the Rossby number to grow and thus further strengthening the easterlies (Schneider and Bordoni 2008; Bordoni and Schneider 2008). At the ascending edge, the seasonality is somewhat complicated, though local minima featuring the smallest Rossby number values, ~0.1, coincide with its poleward-most extents in either summer hemisphere. All together, the meridional variations in the Rossby number within the Hadley cells are smallest and nonmonotonic in latitude within both cells within either summer hemisphere, whereas they decrease sharply and nearly monotonically moving poleward from the equator within either winter hemisphere.

Despite this meridional structure in the local Rossby number, treating it as uniform within each cell results in surprisingly accurate zonal wind fields. Figure 3d shows this for June, and for completeness, Figs. A1 and A2 in the appendix show results for the annual mean, all four seasons, and all 12 calendar months. In all cases, within the span of each Hadley cell, the uniform Rossby number zonal wind field corresponds fairly well with the actual zonal wind field. Two limitations of the u_{Ro} field's accuracy are not capturing the leveling off of the zonal wind in the vicinity of the subtropical jets and, for November–February, being incapable of capturing the superrotation, i.e., positive equatorial zonal wind (Zhang and Lutsko 2022), since u_{Ro} cannot exceed zero at the equator.

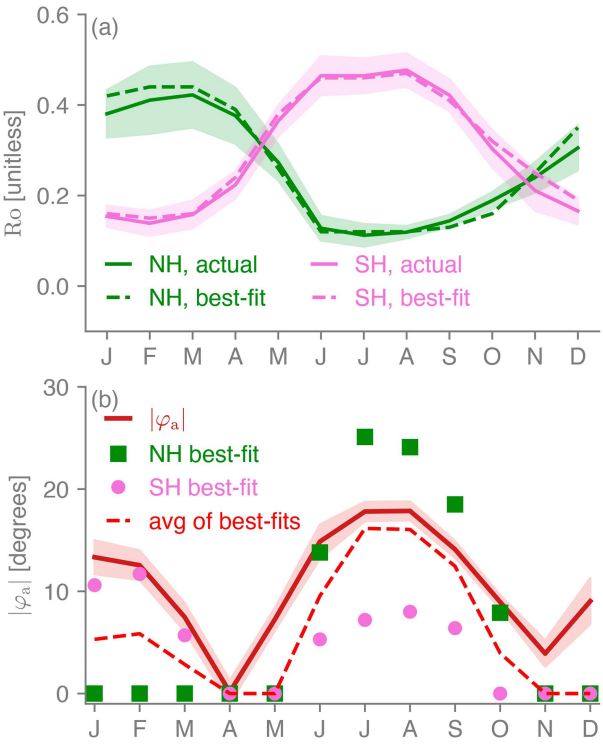

FIG. 5. (a) Seasonal cycles of cell-mean Ro. Solid curves are the climatological values diagnosed directly from ERA5, with the ±1 standard deviation range shaded, and dashed curves are the values for the given month corresponding to the best-fit u_{Ro} field against the ERA5 u. (b) Seasonal cycle of $|\varphi_a|$ in solid red, with the ±1 standard deviation range shaded. Pink dots and green squares are the values corresponding to the SH and NH best-fit u_{Ro} fields, respectively, and the dashed red is their average.

Moreover, for each month, the Rossby number value generating this best fit to the zonal winds is close to the actual cell-mean Rossby number, as shown in Fig. 5a. Both best-fit and actual cell-mean Rossby number values are strongly seasonal, ranging from ~0.1 in either summer cell to ~0.2–0.3 in the equinoctial cells, and up to ~0.4–0.5 in the cross-equatorial solsticial cells. The increase in the Rossby number in either hemisphere from summer to winter reflects the transition from a regime in which eddy stresses prevail throughout the cell, reducing the Rossby number, to one where, as noted above, easterlies in the cross-equatorial cell shield low latitudes from these eddies, enabling the local Rossby number to increase (Schneider and Bordoni 2008; Bordoni and Schneider 2008).

We have also computed the maximum of the local Rossby number within each Hadley cell, over the same span of latitudes in each case as used to compute the cell-mean value. The cell-maximum Rossby number reaches up to 0.65 for the NH in March and 0.79 for the SH in August, and for both cells, it is very highly correlated with the cell-mean

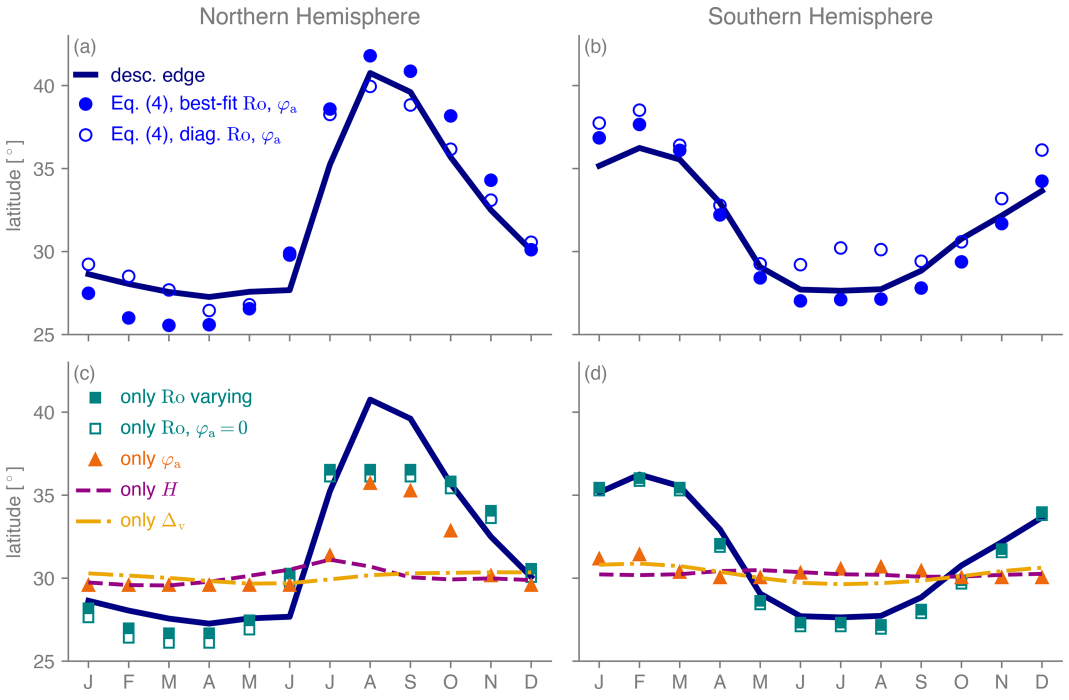

FIG. 6. Climatological monthly seasonal cycle of φ_d in ERA5 in the (a) NH and (b) SH. Solid navy is the actual field, and blue dots are our theoretical prediction using (4), with the values of Ro and φ_a in each month coming from either the best-fit u_{Ro} fields (filled dots) or directly diagnosed (unfilled). In (c) and (d), additional curves use (4) but with all terms except the specified one held constant to their average value across months. For the NH, a lag of 1 month has been applied to all theoretical predictions.

value: $r = 0.967$ for the NH and $r = 0.996$ for the SH (not shown).

Figure 5b shows the monthly climatologies of the ascending edge poleward displacement, the corresponding values for each of the NH and SH from the best-fit u_{Ro} fields, and the average of these NH and SH values. The best-fit ascending edge displacements broadly agree with the corresponding diagnosed values, albeit less cleanly than for the best-fit versus cell-mean Rossby numbers. The actual $|\varphi_a|$ expands poleward and contracts equatorward twice over the seasonal cycle, moving as far poleward as ~18° in boreal summer and ~13° in austral summer. The best-fit values are closest to this in either summer hemisphere, and the average of the best-fit values in either hemisphere in each month is equatorward but otherwise comparable to the actual. The NH best-fit ascending edge reaches as far as 25.1°N during boreal summer, which likely results from the regional monsoons, especially the Indian summer monsoon, which enables ascent regionally to extend deeper into the subtropics (e.g., Nie et al. 2010).

We conclude from these diagnostics that a uniform Rossby number approximation, though poor for the Rossby number itself, yields useful fields for our purposes: u_{Ro} captures the actual upper-branch zonal winds fairly well, with the corresponding Ro and $|\varphi_a|$ values being consistent with the diagnosed ones. We therefore proceed using the u_{Ro}-based theory for the descending edge based on baroclinic instability onset.

Figures 6a and 6b show the seasonal cycles of the NH and SH descending edges and their predictions using (4). Two predictions are shown for each hemisphere, one using the best-fit values and one using the diagnosed values for Ro and $|\varphi_a|$. For the NH only, these include an empirical 1-month lag to the predictions, as Hill et al. (2022) also required for both hemispheres in an idealized aquaplanet. Our theory captures the seasonal cycle of the descending edge in each hemisphere well. It performs slightly better using the best-fit rather than diagnosed Ro and φ_a values for the SH, but vice versa for the NH.

Given this accuracy, we can evaluate the relative importance of each term by holding all terms in (4) constant at their average values across months except one that remains fully varying, with the results shown in Figs. 6c and 6d. These use the bestfit rather than diagnosed values for the Rossby number and ascending edge, but this makes little difference (not shown). The seasonal cycles of the midlatitude tropopause heights and static stabilities matter very little. This is partly because their own seasonal cycles are both small, varying by at most a few percent from their averages across months (not shown). Fractional variations in the ascending edge displacement are larger, yet its seasonality also plays a mostly modest role, with a substantial contribution only to the NH descending edge in late boreal summer through autumn when it helps to push the descending edge to its most poleward values. It is the Rossby number seasonality that predominantly controls the seasonal cycles of the descending edges in both hemispheres, with the predictions weakly modified when the seasonality in all other terms is removed. For the SH, if anything the fit improves slightly when the other terms are held fixed.

In addition to the ascending edge seasonality being unimportant, its annual-mean displacement is modest enough that setting $\varphi_a = 0$ only weakly modifies the descending edge predictions (unfilled squares in Fig. 6). In that case, (4) reduces to (6), from which it follows that the descending edges should vary as $\mathrm{Ro}^{-1/4}$. The exponents estimated from linear regression in log–log space between the diagnosed $|\varphi_d|$ and cell-mean Ro are fairly close to this: again with the 1-month empirical lag applied for the NH only, the values for the NH and SH are −0.25 and −0.23, respectively, using the best-fit Ro values or −0.28 and −0.21 using the diagnosed cell-mean Ro values.

For the NH cell during local summer–autumn, it may seem curious that, on the one hand, including φ_a variations alone captures much of the behavior of the descending edge, yet on the other hand, setting $\varphi_a = 0$ makes little difference when only Ro is allowed to vary. We reconcile these results by examining the partial derivatives of (4). Ignoring the c_d constant for simplicity, these are

$$\frac{\partial \varphi_d^2}{\partial \mathrm{Ro}} \approx -\frac{\varphi_{d,0}^4}{2\mathrm{Ro}}\left(\frac{\varphi_a^4}{4} + \varphi_{d,0}^4\right)^{-1/2},$$

$$\frac{\partial \varphi_d^2}{\partial \varphi_a} \approx \varphi_a\left[1 + \frac{\varphi_a^2}{2}\left(\frac{\varphi_a^4}{4} + \varphi_{d,0}^4\right)^{-1/2}\right].$$

If we further treat $2^{-1/2}|\varphi_a| \ll \varphi_{d,0}$, which though imperfect seems fair enough for these purposes, these reduce to

$$\frac{\partial \varphi_d^2}{\partial \mathrm{Ro}} \approx -\frac{\varphi_{d,0}^2}{2\mathrm{Ro}},$$

$$\frac{\partial \varphi_d^2}{\partial \varphi_a} \approx \varphi_a,$$

from which it is clear that φ_d is considerably more sensitive to variations in Ro than to variations in φ_a.

5. Interannual variability

We now show that the main results just presented for the climatological seasonal cycle also hold for interannual variability of both hemispheres' annual-mean cells: the Hadley cell upper-branch zonal wind fields are well captured by u_{Ro}, the descending edge variations are well captured by (4), and within (4), the cell-mean Rossby number is the most influential term.

Figure 7 shows the time series of the NH and SH descending edges, NH and SH cell-mean Rossby numbers, and the shared ascending edge, each computed from the annual-mean streamfunction for each calendar year, 1979–2023. Both the mean and variance of each descending edge is similar between the hemispheres: means 30.3°N and 31.0°S and interannual standard deviations 0.49° for the NH and 0.43° for the SH. The covariation of the two descending edges is modest, with correlation coefficient $r = 0.30$. As for the seasonal cycle, the interannual edge displacements do not strongly depend on the metric used; comparing our definitions to the 500-hPa

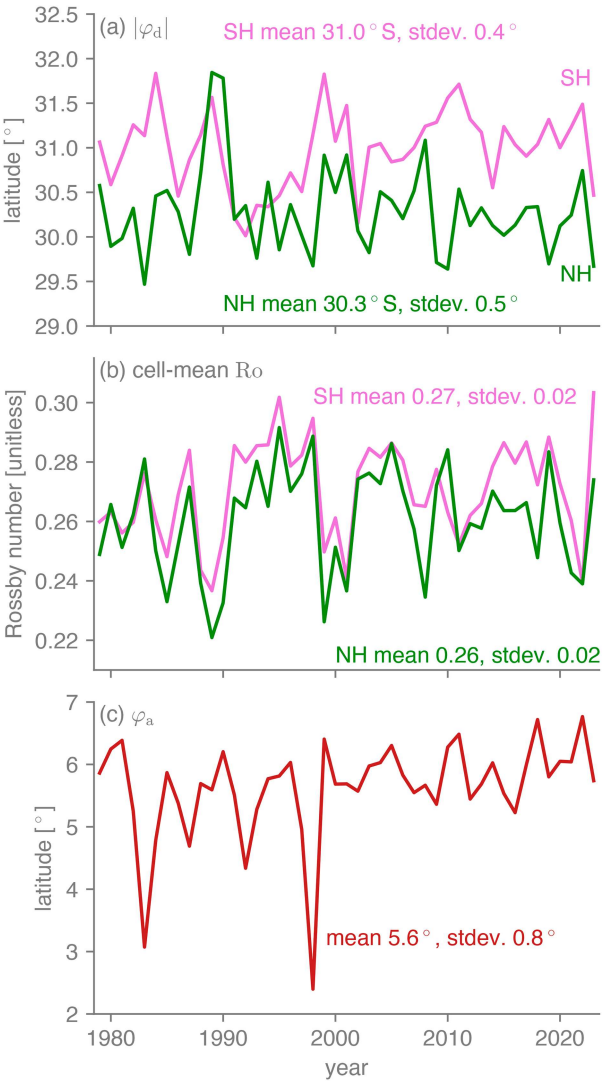

FIG. 7. Time series spanning 1979–2023 of annual-mean values of (a) NH and SH Hadley cell descending edges, (b) NH and SH cell-mean Rossby numbers, and (c) the shared ascending edge.

zero crossing, the correlation coefficients for the NH descending edge, ascending edge, and SH descending edge are 0.87, 0.95, and 0.96, respectively (not shown).

For each year, we compute best-fit u_{Ro} profiles and corresponding best-fit Rossby number and ascending edge values for each Hadley cell for that year, following the same methodology as for the climatological seasonal cycle described above. The uniform Rossby approximations capture the upper-tropospheric zonal winds within the Hadley cells reasonably well, which Fig. 8a shows for the year 1999, selected quasi-randomly, as one example and with the fits comparably accurate in all other years (not shown). Figure 8b shows the best-fit and actual cell-mean Rossby numbers for each year plotted against one another; they are very highly correlated, $r = 0.94$ and 0.95 for the NH and SH, respectively, and fall close to the one-to-one line. In contrast and unlike for the seasonal cycle,

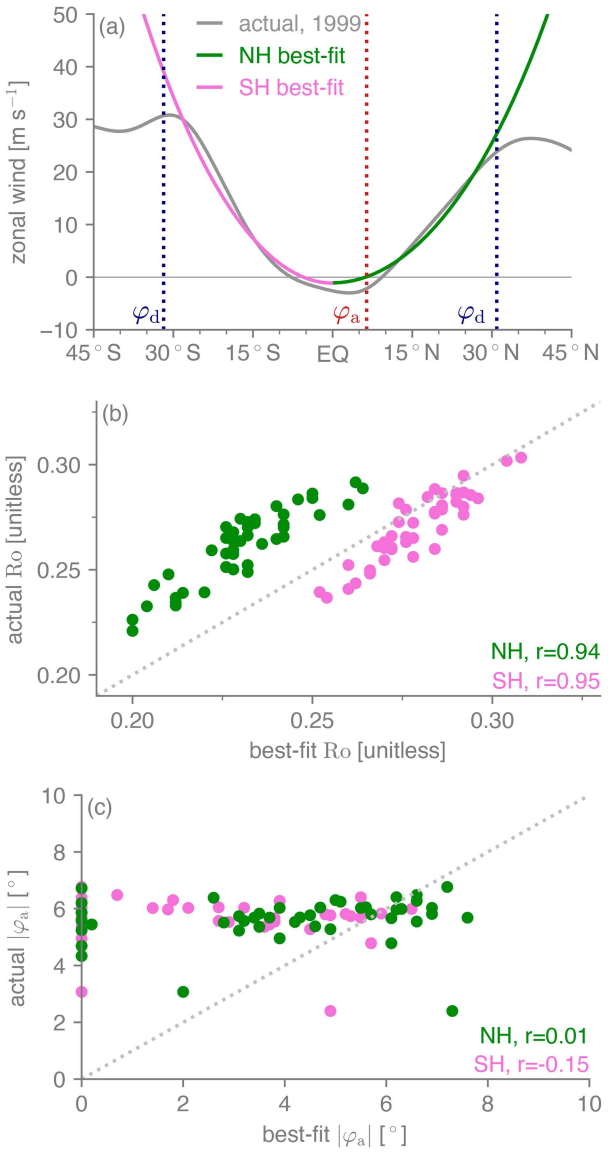

FIG. 8. (a) For the year 1999, actual 200-hPa zonal wind and corresponding best-fit u_{Ro} field (gray) for the SH (pink) and NH (green) Hadley cell, with the Hadley cell edges overlaid as vertical dotted lines. (b) Scatterplot of best-fit vs. diagnosed cell-mean Rossby number in each year for the SH (pink) and NH (green) cells. The corresponding Pearson's correlation coefficient for each hemisphere is also printed, and the dotted gray diagonal line is the one-to-one line. (c) As in (b), but for the best-fit vs. diagnosed ascending edge displacement rather than the Rossby number.

there is almost no correspondence between the actual and best-fit values for the ascending edge displacement, as shown in Fig. 8c. This implies that interannual variations in the annual-mean zonal wind in the Hadley cell upper branches depend weakly on interannual variations of the ascending edge (Fig. 7c). This is consistent in sign with the annual-mean φ_a itself being small, given that from (2), we have $\partial u_{Ro}/\partial\varphi_a = -2\mathrm{Ro}\Omega a\varphi_a$, i.e., that the change in u_{Ro} with respect to φ_a is proportional to φ_a itself.

We then use (4) to predict the descending edge of each cell in each year using these best-fit values of Ro and $|\varphi_a|$ and diagnosed values of the midlatitude tropopause heights and static stabilities, with as noted c_d values of 1.02 for the NH and 1.09 for the SH. Figure 9a shows the results. Our theory performs fairly well, $r = 0.75$ and 0.66 for the NH and SH, respectively, though it clearly leaves more variability unexplained than in the seasonal cycle case. Unlike the seasonal cycle, the theory performs somewhat better overall for the NH compared to the SH. As expected for annual averages, no empirical lag is required for either hemisphere. Results are similar using the diagnosed rather than best-fit Ro and $|\varphi_a|$ values: $r = 0.77$ and 0.57 between the prediction and the actual edge for the NH and SH, respectively.

As for the seasonal cycle, the variations in Ro predominate over changes in all other fields in setting the descending edge. This can be seen in Figs. 9b and 9c, which show the predicted versus actual descending edges in each year when either (Fig. 9b) Ro is the only term varying or (Fig. 9c) Ro is the only term *not* varying. In fact, the fits are slightly improved when the factors other than the Rossby number are held constant ($r = 0.80$ and 0.67 for NH and SH, respectively), as the relationship between the descending edges and all the other factors combined, though weak, are of the wrong sign for both hemispheres ($r = -0.32$ and -0.13 for NH and SH, respectively). This stems from the tropopause height: The descending edges are negatively correlated with the midlatitude tropopause height in the same hemisphere (not shown). However, this is sensitive to the definition of the midlatitude band; when fixed boundaries are used instead, e.g., 40°–60°, the correlations become insignificant. In any case, by any metric, the midlatitude tropopause height is not an important factor.

The influence of each factor can be understood as follows. The midlatitude tropopause heights and static stabilities simply do not change much from year to year: none varies by more than ±3% for any year 1979–2023 from its climatological value (not shown). Over the same period, the cell-mean Rossby numbers vary by as much as ±15%. For the ascending edge displacement, though fractional variations from year to year can exceed ~50%, in absolute terms, these displacements are smaller than those during the seasonal cycle—minimum and maximum values across all years are 2.4° and 6.8°, respectively, compared to corresponding seasonal cycle values of 0.1° and 17.7°—in which context also they play a minor role compared to Rossby number variations.

This predominance of the Rossby number means that, again as for the seasonal cycle, the full expression (4) can be effectively replaced with the on-equatorial-ascent case (6), yielding an expected power-law exponent of −1/4 for Ro against each descending edge. The power-law exponents estimated from the log–log regression of φ_d against Ro are somewhat lower than, but in the ballpark of, this −0.25 value: −0.19 for the NH and −0.21 for the SH using the best-fit Ro or −0.19 and −0.15 using the diagnosed cell-mean Ro.

The Rossby numbers for the NH and SH cells (Fig. 7b) are highly correlated with one another ($r = 0.84$), indicating that interannual variations in the eddy stresses tend to be coherent

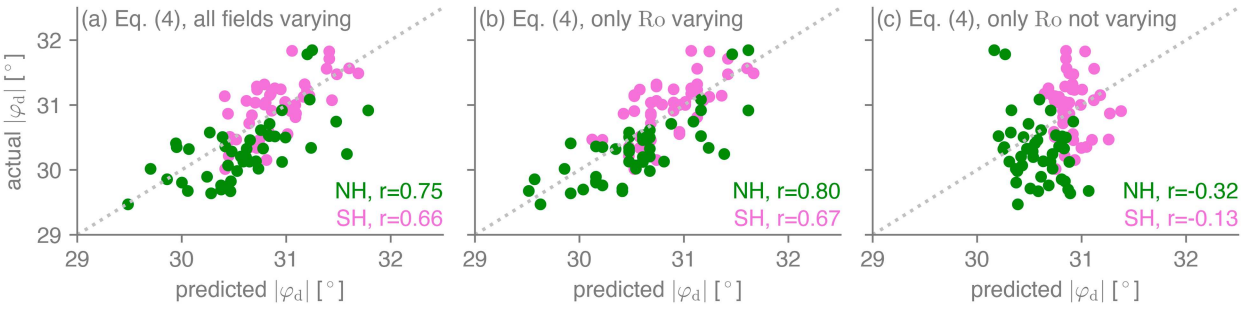

FIG. 9. (a) Descending edge predicted by (4) for each year using diagnosed values of all terms for that year and cell vs. the actual descending edge for that year and cell. (b) As in (a), but with all fields except Ro set to their climatological values. (c) As in (a), but with only Ro set to its climatological value.

across the tropics, evocative of the tropics-wide influence of ENSO (Lu et al. 2008). Figure 10 provides an interannual correlation heat map of the diagnosed cell-mean Rossby numbers, descending edges, ascending edge displacement, and the standard Niño-3.4 index, with all correlations computed using linearly detrended fields. Consistent in sign with our arguments and the existing literature regarding ENSO, El Niño conditions (i.e., positive Niño-3.4) act to contract all three Hadley cell edges equatorward and increase both cell-mean Rossby numbers. Conversely, the SH descending edge has virtually no linear relationship with the ascending edge ($r = 0.06$). While prior literature has argued that the ENSO relationships with the Hadley cells are tighter for the SH than for the NH (Hasan et al. 2024), with the Arctic Oscillation playing a comparable role to ENSO for the NH (Seo et al. 2023), the difference between the hemispheres we find in this regard is modest, with $r = -0.47$ versus -0.54 between Niño-3.4 and the descending edge for the NH and SH, respectively.

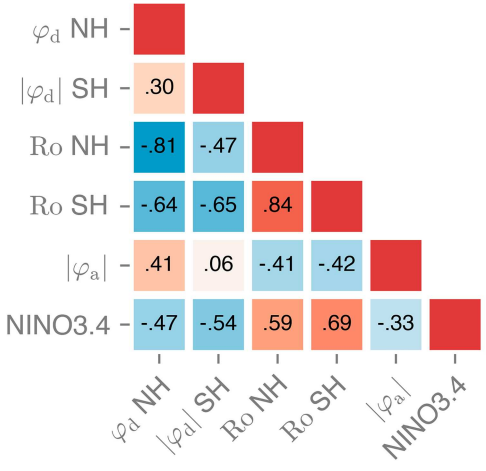

FIG. 10. Heat map of Pearson correlation coefficients among various metrics of the NH and SH Hadley cells as well as the Niño-3.4 index, all annual means. From top to bottom and left to right in each panel, the quantities are NH cell-mean Ro, SH cell-mean Ro, NH φ_d, $|\varphi_a|$, SH $-\varphi_d$, and the Niño-3.4 index. All quantities are computed over 1979–2023 and linearly detrended over that period prior to the computation of correlations.

Both cell-mean Rossby numbers decrease as the ascending edge moves farther off equator ($r = -0.41$ and -0.42 for the NH and SH, respectively), whereas for the seasonal cycle, the poleward migration of $|\varphi_a|$ acts to increase Ro within the cross-equatorial cell by generating stronger and more extensive easterlies that shield the deep tropics from extratropical wave breaking (Schneider and Bordoni 2008). In the annual mean, the SH cell is modestly cross equatorial, and so by this mechanism alone, the SH cell-mean Rossby number would be positively rather than negatively correlated with the ascending edge displacement. Arguably, this mechanism becomes salient only once the cell becomes even more monsoonal, and a more compelling explanation lies in ENSO: In El Niño years, the anomalous surface warmth in the eastern equatorial Pacific directly pulls the ascent equatorward (e.g., Adam et al. 2016) and also, through mechanisms we are less certain of, enables the Rossby number within the tropics to grow.

6. Conclusions

We conclude that both the climatological seasonal cycle and interannual variations of Earth's poleward, descending Hadley cell edges can be usefully interpreted via the simple two-layer, quasigeostrophic baroclinic instability expression (4), in which crucially the upper-branch zonal wind profile used within either cell is the uniform Rossby number solution (2). The value of this uniform Rossby number amounts to a cell-mean value of the local Rossby number across each cell's upper branch. And of the terms appearing in (4), this cell-mean Rossby number predominantly controls seasonal and interannual variations of both hemispheres' descending edges.

With these results from ERA5, the uniform Ro framework for the descending edges encapsulated into (4) has now proven successful for two distinct regimes of Hadley cell seasonality. Hill et al. (2022) originally test the theory using a seasonally forced aquaplanet simulation with a rather shallow, 10-m ocean mixed layer depth. As a result, the Hadley cells—though Earth-like in their overall meridional extent—are Mars-like in their seasonality (Zalucha et al. 2010): φ_a migrates abruptly and deeply into either summer hemisphere just after either equinox, so much so that φ_a rather than Ro predominantly controls the descending edge migrations. The theory's dexterity

across these regimes suggests it could be useful for the Hadley cells of terrestrial atmospheres broadly.

At the same time, in addition to lacking a predictive theory for Ro—which, for Earth at least, is the central parameter—we do not understand why the theory's predictions lead the actual descending edge by 1 month in the NH only. It can be inferred from Peles and Lachmy (2023, cf. their Fig. 6) that multiple other metrics of the lowest latitude of baroclinic growth also lead the Hadley cell descending edge by roughly one month in the NH but not the SH. This suggests roots in something other than the precise physical assumptions we have made. The same lag is required in the Hill et al. (2022) aquaplanet case just described—meaning, somewhat curiously, it is the case with the largest heat capacity—Earth's SH, in which the descending edge is more in phase with these environmental influences. Hill et al. (2022) also speculate about the finite time scale of Rossby wave generation in the extratropics followed by equatorward propagation and breaking; for that mechanism to be relevant here, wave generation and propagation would need to occur more slowly in the NH than SH. Analysis of idealized simulations with differing mixed layer depths between the two hemispheres or idealized continents (e.g., Maroon et al. 2016; Voigt et al. 2016; Hui and Bordoni 2021) would help shed light on all this.

Notably uninfluential both seasonally and interannually is the midlatitude static stability, which under global warming is projected to increase and, through appeal to (6), thereby predominantly drive the poleward expansion of the descending edges (e.g., Kang and Lu 2012; Chemke and Polvani 2019). To our knowledge, no study has yet investigated the role of the cell-mean Rossby numbers in warming-driven Hadley cell expansion; Kang and Lu (2012) find large seasonal differences in the climatological value of a bulk Rossby number for each Hadley cell, but they neglect any changes to these bulk Rossby numbers as the planet warms. All else equal, an increase in the Rossby number would retract the descending edge, while a decrease would expand the descending edge poleward. The influence of the Rossby number on Hadley cell expansion with global warming could also come from the Rossby number's climatological value rather than its own response to warming: by (6), an atmosphere with larger climatological cell-mean Rossby numbers would migrate less for a given change in any of the other terms, compared to a model with smaller climatological cell-mean Rossby numbers. Given that multimodel-mean projections under high-CO_2 forcing are robustly of expansion of the descending edges (e.g., Grise and Davis 2020), possibilities include that the cell-mean Rossby numbers are increasing, that they are decreasing but not enough to counter the increased subtropical static stability, or that the framework simply does not work in this context.

Acknowledgments. We thank Isaac Held for useful discussions of this work. S. A. H. acknowledges funding from the NSF Climate and Large-scale Dynamics program, Award AGS-2411723. J. L. M. acknowledges funding from the NSF Climate and Large-scale Dynamics program, Award AGS-1912673. S. B. acknowledges partial support from the European Union under Next-Generation EU, Mission 4 Component 2—CUP E53D23021930001 and Next-Generation EU, Mission 4 Component 2–CUP E63C22000970007.

Data availability statement. ERA5 data are available for free, public download at https://www.ecmwf.int/en/forecasts/dataset/ecmwf-reanalysis-v5.

APPENDIX

Uniform Rossby Number Zonal Wind Fields Compared to Actual Fields

For completeness, Fig. A1 shows the diagnosed ERA5 200-hPa zonal wind and corresponding best-fit u_{Ro} fields computed for the climatological annual mean and for each meteorological season, and Fig. A2 shows the same for each calendar month.

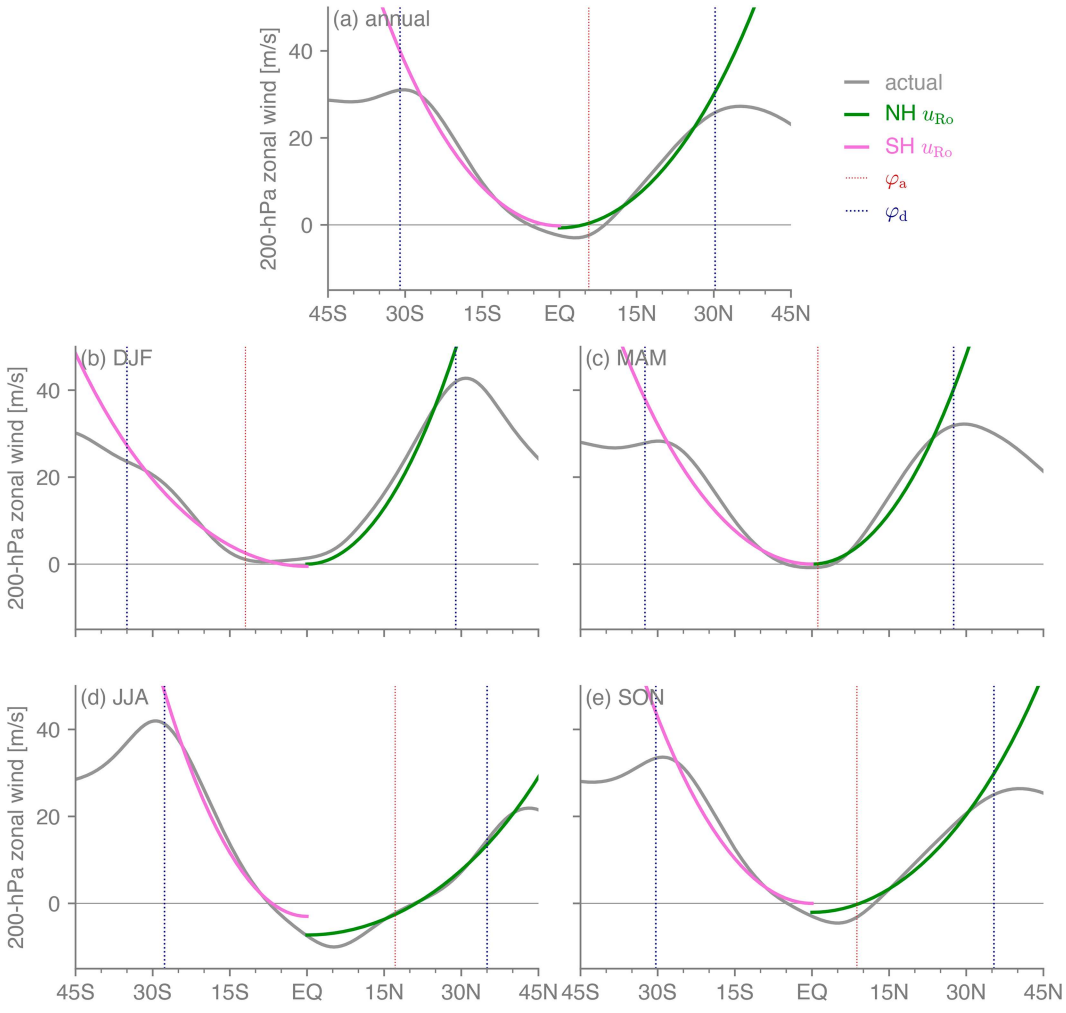

FIG. A1. For the (a) annual and (b)–(e) seasonal climatologies, 200-hPa zonal wind and best-fit uniform Ro zonal wind fields (gray) for the SH (pink) and NH (green) Hadley cell, restricting to that hemisphere. Overlaid red and blue dotted vertical lines are the diagnosed ascending and descending edges, respectively.

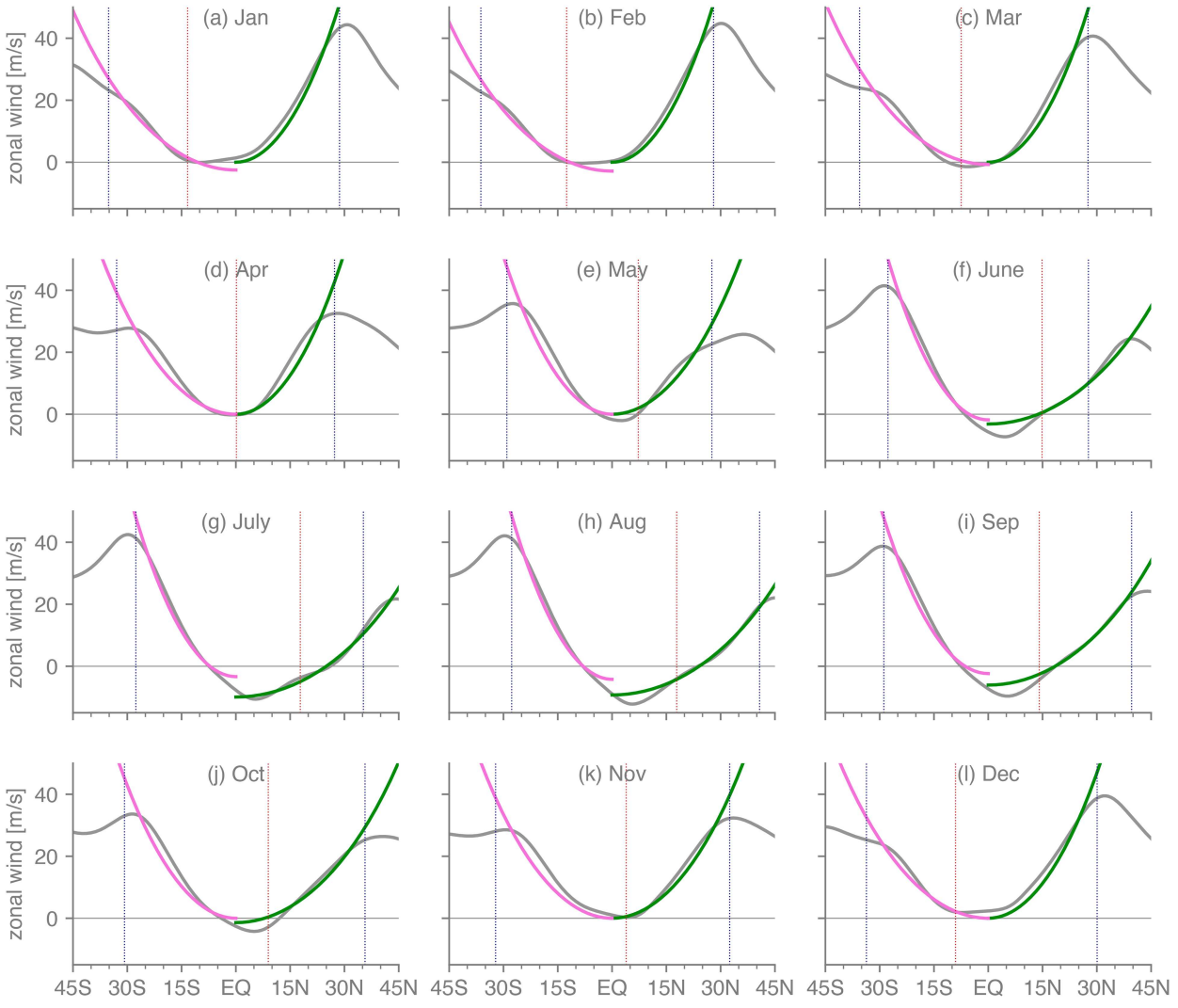

FIG. A2. As in Fig. A1, but for each calendar month.

REFERENCES

Adam, O., T. Bischoff, and T. Schneider, 2016: Seasonal and interannual variations of the energy flux equator and ITCZ. Part I: Zonally averaged ITCZ position. *J. Climate*, **29**, 3219–3230, https://doi.org/10.1175/JCLI-D-15-0512.1.

——, and Coauthors, 2018: The TropD software package (v1): Standardized methods for calculating tropical-width diagnostics. *Geosci. Model Dev.*, **11**, 4339–4357, https://doi.org/10.5194/gmd-11-4339-2018.

Bordoni, S., and T. Schneider, 2008: Monsoons as eddy-mediated regime transitions of the tropical overturning circulation. *Nat. Geosci.*, **1**, 515–519, https://doi.org/10.1038/ngeo248.

Caballero, R., 2007: Role of eddies in the interannual variability of Hadley cell strength. *Geophys. Res. Lett.*, **34**, L22705, https://doi.org/10.1029/2007GL030971.

Chemke, R., and L. M. Polvani, 2019: Exploiting the abrupt $4 \times CO_2$ scenario to elucidate tropical expansion mechanisms. *J. Climate*, **32**, 859–875, https://doi.org/10.1175/JCLI-D-18-0330.1.

Chen, G., and I. M. Held, 2007: Phase speed spectra and the recent poleward shift of Southern Hemisphere surface westerlies. *Geophys. Res. Lett.*, **34**, L21805, https://doi.org/10.1029/2007GL031200.

Davis, N. A., and T. Birner, 2022: Eddy-mediated Hadley cell expansion due to axisymmetric angular momentum adjustment to greenhouse gas forcings. *J. Atmos. Sci.*, **79**, 141–159, https://doi.org/10.1175/JAS-D-20-0149.1.

Dima, I. M., and J. M. Wallace, 2003: On the seasonality of the Hadley cell. *J. Atmos. Sci.*, **60**, 1522–1527, https://doi.org/10.1175/1520-0469(2003)060<1522:OTSOTH>2.0.CO;2.

Ferrel, W., 1856: An essay on the winds and the currents of the ocean. *Nashville J. Med. Surg.*, **11**, 287–301.

Geen, R., F. H. Lambert, and G. K. Vallis, 2019: Processes and timescales in onset and withdrawal of "aquaplanet monsoons". *J. Atmos. Sci.*, **76**, 2357–2373, https://doi.org/10.1175/JAS-D-18-0214.1.

Grise, K. M., and S. M. Davis, 2020: Hadley cell expansion in CMIP6 models. *Atmos. Chem. Phys.*, **20**, 5249–5268, https://doi.org/10.5194/acp-20-5249-2020.

Hadley, G., 1735: VI. Concerning the cause of the general trade-winds. *Philos. Trans. Roy. Soc.*, **39**, 58–62, https://doi.org/10.1098/rstl.1735.0014.

Halley, E., 1686: An historical account of the trade winds, and monsoons, observable in the seas between and near the tropicks, with an attempt to assign the physical cause of the said winds. *Philos. Trans. Roy. Soc.*, **16**, 153–168, https://doi.org/10.1098/rstl.1686.0026.

Hasan, M., S. M. Larson, K. McMonigal, W. A. Robinson, and A. Aiyyer, 2024: Hemisphere-dependent impacts of ENSO and atmospheric eddies on Hadley circulation. *J. Climate*, **37**, 6533–6548, https://doi.org/10.1175/JCLI-D-24-0112.1.

Held, I. M., 1978: The vertical scale of an unstable baroclinic wave and its importance for eddy heat flux parameterizations. *J. Atmos. Sci.*, **35**, 572–576, https://doi.org/10.1175/1520-0469(1978)035<0572:TVSOAU>2.0.CO;2.

——, 2000: The general circulation of the atmosphere: 2000 program in geophysical fluid dynamics. WHOI Tech. Rep. WHOI-2001-03, 54 pp., https://gfd.whoi.edu/wp-content/uploads/sites/18/2018/07/previous_announcement2000_16868.pdf.

——, and A. Y. Hou, 1980: Nonlinear axially symmetric circulations in a nearly inviscid atmosphere. *J. Atmos. Sci.*, **37**, 515–533, https://doi.org/10.1175/1520-0469(1980)037<0515:NASCIA>2.0.CO;2.

Hersbach, H., and Coauthors, 2020: The ERA5 global reanalysis. *Quart. J. Roy. Meteor. Soc.*, **146**, 1999–2049, https://doi.org/10.1002/qj.3803.

Hilgenbrink, C. C., and D. L. Hartmann, 2018: The response of Hadley circulation extent to an idealized representation of poleward ocean heat transport in an aquaplanet GCM. *J. Climate*, **31**, 9753–9770, https://doi.org/10.1175/JCLI-D-18-0324.1.

Hill, S. A., S. Bordoni, and J. L. Mitchell, 2021: Solsticial Hadley cell ascending edge theory from supercriticality. *J. Atmos. Sci.*, **78**, 1999–2011, https://doi.org/10.1175/JAS-D-20-0341.1.

——, ——, and ——, 2022: A theory for the Hadley cell descending and ascending edges throughout the annual cycle. *J. Atmos. Sci.*, **79**, 2515–2528, https://doi.org/10.1175/JAS-D-21-0328.1.

Huang, B., and Coauthors, 2015: Extended Reconstructed Sea Surface Temperature version 4 (ERSST.v4). Part I: Upgrades and intercomparisons. *J. Climate*, **28**, 911–930, https://doi.org/10.1175/JCLI-D-14-00006.1.

Hui, K. L., and S. Bordoni, 2021: Response of monsoon rainfall to changes in the latitude of the equatorward coastline of a zonally symmetric continent. *J. Atmos. Sci.*, **78**, 1429–1444, https://doi.org/10.1175/JAS-D-20-0110.1.

Kang, S. M., and J. Lu, 2012: Expansion of the Hadley cell under global warming: Winter versus summer. *J. Climate*, **25**, 8387–8393, https://doi.org/10.1175/JCLI-D-12-00323.1.

Korty, R. L., and T. Schneider, 2008: Extent of Hadley circulations in dry atmospheres. *Geophys. Res. Lett.*, **35**, L23803, https://doi.org/10.1029/2008GL035847.

Levine, X. J., and T. Schneider, 2011: Response of the Hadley circulation to climate change in an aquaplanet GCM coupled to a simple representation of ocean heat transport. *J. Atmos. Sci.*, **68**, 769–783, https://doi.org/10.1175/2010JAS3553.1.

——, and ——, 2015: Baroclinic eddies and the extent of the Hadley circulation: An idealized GCM study. *J. Atmos. Sci.*, **72**, 2744–2761, https://doi.org/10.1175/JAS-D-14-0152.1.

Lindzen, R. S., and A. V. Hou, 1988: Hadley circulations for zonally averaged heating centered off the equator. *J. Atmos. Sci.*, **45**, 2416–2427, https://doi.org/10.1175/1520-0469(1988)045<2416:HCFZAH>2.0.CO;2.

Lu, J., G. Chen, and D. M. W. Frierson, 2008: Response of the zonal mean atmospheric circulation to El Niño versus global warming. *J. Climate*, **21**, 5835–5851, https://doi.org/10.1175/2008JCLI2200.1.

Maroon, E. A., D. M. W. Frierson, S. M. Kang, and J. Scheff, 2016: The precipitation response to an idealized subtropical continent. *J. Climate*, **29**, 4543–4564, https://doi.org/10.1175/JCLI-D-15-0616.1.

Mitchell, J. L., G. K. Vallis, and S. F. Potter, 2014: Effects of the seasonal cycle on superrotation in planetary atmospheres. *Astrophys. J.*, **787**, 23, https://doi.org/10.1088/0004-637X/787/1/23.

Nie, Ji., W. R. Boos, and Z. Kuang, 2010: Observational evaluation of a convective quasi-equilibrium view of monsoons. *Journal of Climate*, **23**, 4416–4428, https://doi.org/10.1175/2010JCLI3505.1.

Peles, O., and O. Lachmy, 2023: Estimating the lowest latitude of baroclinic growth. *J. Atmos. Sci.*, **80**, 1401–1414, https://doi.org/10.1175/JAS-D-22-0201.1.

Schneider, T., 2006: The general circulation of the atmosphere. *Annu. Rev. Earth Planet. Sci.*, **34**, 655–688, https://doi.org/10.1146/annurev.earth.34.031405.125144.

——, and S. Bordoni, 2008: Eddy-mediated regime transitions in the seasonal cycle of a Hadley circulation and implications for monsoon dynamics. *J. Atmos. Sci.*, **65**, 915–934, https://doi.org/10.1175/2007JAS2415.1.

Seo, K.-H., S.-P. Yoon, J. Lu, Y. Hu, P. W. Staten, and D. M. W. Frierson, 2023: What controls the interannual variation of Hadley cell extent in the Northern Hemisphere: Physical mechanism and empirical model for edge variation. *npj Climate Atmos. Sci.*, **6**, 204, https://doi.org/10.1038/s41612-023-00533-w.

Showman, A. P., R. D. Wordsworth, T. M. Merlis, and Y. Kaspi, 2014: Atmospheric circulation of terrestrial exoplanets. *Comparative Climatology of Terrestrial Planets*, 2nd ed. S. J. Mackwell et al., Eds., University of Arizona Press, 277–326.

Singh, M. S., 2019: Limits on the extent of the solsticial Hadley cell: The role of planetary rotation. *J. Atmos. Sci.*, **76**, 1989–2004, https://doi.org/10.1175/JAS-D-18-0341.1.

Sobel, A. H., and T. Schneider, 2009: Single-layer axisymmetric model for a Hadley circulation with parameterized eddy momentum forcing. *J. Adv. Model. Earth Syst.*, **1**, 10, https://doi.org/10.3894/JAMES.2009.1.10.

Staten, P. W., and Coauthors, 2020: Tropical widening: From global variations to regional impacts. *Bull. Amer. Meteor. Soc.*, **101**, E897–E904, https://doi.org/10.1175/BAMS-D-19-0047.1.

Tandon, N. F., E. P. Gerber, A. H. Sobel, and L. M. Polvani, 2013: Understanding Hadley cell expansion versus contraction: Insights from simplified models and implications for recent observations. *J. Climate*, **26**, 4304–4321, https://doi.org/10.1175/JCLI-D-12-00598.1.

Vallis, G. K., P. Zurita-Gotor, C. Cairns, and J. Kidston, 2015: Response of the large-scale structure of the atmosphere to global warming. *Quart. J. Roy. Meteor. Soc.*, **141**, 1479–1501, https://doi.org/10.1002/qj.2456.

Voigt, A., and Coauthors, 2016: The tropical rain belts with an annual cycle and a continent model intercomparison project: TRACMIP. *J. Adv. Model. Earth Syst.*, **8**, 1868–1891, https://doi.org/10.1002/2016MS000748.

Walker, C. C., and T. Schneider, 2005: Response of idealized Hadley circulations to seasonally varying heating. *Geophys. Res. Lett.*, **32**, L06813, https://doi.org/10.1029/2004GL022304.

——, and ——, 2006: Eddy influences on Hadley circulations: Simulations with an idealized GCM. *J. Atmos. Sci.*, **63**, 3333–3350, https://doi.org/10.1175/JAS3821.1.

Watt-Meyer, O., and D. M. W. Frierson, 2019: ITCZ width controls on Hadley cell extent and eddy-driven jet position and their response to warming. *J. Climate*, **32**, 1151–1166, https://doi.org/10.1175/JCLI-D-18-0434.1.

——, ——, and Q. Fu, 2019: Hemispheric asymmetry of tropical expansion under CO_2 forcing. *Geophys. Res. Lett.*, **46**, 9231–9240, https://doi.org/10.1029/2019GL083695.

Wei, H.-H., and S. Bordoni, 2018: Energetic constraints on the ITCZ position in idealized simulations with a seasonal cycle. *J. Adv. Model. Earth Syst.*, **10**, 1708–1725, https://doi.org/10.1029/2018MS001313.

WMO, 1957: Meteorology—A three-dimensional science. *WMO Bull.*, **6**, 134–138.

Zalucha, A. M., R. A. Plumb, and R. J. Wilson, 2010: An analysis of the effect of topography on the Martian Hadley cells. *J. Atmos. Sci.*, **67**, 673–693, https://doi.org/10.1175/2009JAS3130.1.

Zhang, P., and N. J. Lutsko, 2022: Seasonal superrotation in Earth's troposphere. *J. Atmos. Sci.*, **79**, 3297–3314, https://doi.org/10.1175/JAS-D-22-0066.1.

Zhou, W., and S.-P. Xie, 2018: A hierarchy of idealized monsoons in an intermediate GCM. *J. Climate*, **31**, 9021–9036, https://doi.org/10.1175/JCLI-D-18-0084.1.

Zurita-Gotor, P., and P. Álvarez-Zapatero, 2018: Coupled interannual variability of the Hadley and Ferrel cells. *J. Climate*, **31**, 4757–4773, https://doi.org/10.1175/JCLI-D-17-0752.1.